AAS 08-056

ORION NAVIGATION SENSITIVITIES TO GROUND STATION INFRASTRUCTURE FOR LUNAR MISSIONS

Joel Getchius[*], Dr. Daniel Kukitschek[†], and Dr. Timothy Crain[‡]

The Orion Crew Exploration Vehicle (CEV) will replace the Space Shuttle and serve as the next-generation spaceship to carry humans to the International Space Station and back to the Moon for the first time since the Apollo program. As in the Apollo and Space Shuttle programs, the Mission Control Navigation team will utilize radiometric measurements to determine the position and velocity of the CEV. In the case of lunar missions, the ground station infrastructure consisting of approximately twelve stations distributed about the Earth and known as the Apollo Manned Spaceflight Network, no longer exists. Therefore, additional tracking resources will have to be allocated or constructed to support mission operations for Orion lunar missions. This paper examines the sensitivity of Orion navigation for lunar missions to the number and distribution of tracking sites that form the ground station infrastructure.

INTRODUCTION

The uncertainty in the navigation architecture for lunar missions is of great concern to the Orion navigation design team. The following analysis takes a look at the sensitivity of the navigation performance with respect to ground station configuration about the TEI-3 maneuver by three methods:

1. A heuristic study on ground station geometrical impacts to navigation
2. A comparison between Deep Space Network only navigation performance and Apollo Manned Spaceflight Network navigation performance
3. An examination of additional "worst-case" trajectories

ASSUMPTIONS AND CONSTRAINTS

Ground Tracking Network

Currently, the only remnants of the Apollo Manned Spaceflight Ground Network (MSFN) is the three Deep Space Navigation (DSN) stations located at Canberra (Australia), Goldstone (California), and Madrid (Spain). However, the Orion project has long had an understanding with Constellation Level 2 that any future navigation architecture will have at least the capabilities of the MSFN. Therefore the main assumption in this analysis is there exists a ground station architecture similar to the MSFN with modern electronics (ie, bias and noise values reflective of current DSN capability). This consists of the network of ground stations, shown in Figure 1 and Table 1, generating concurrent measurements from 3 stations. The measurements generated are:

[*] Title, department, affiliation, address.
[†] Title, department, affiliation, address.
[‡]

1. 2-way range and Doppler from a “master” (transmitting) station
2. 3-way Doppler from the two “slaves” (receive only)

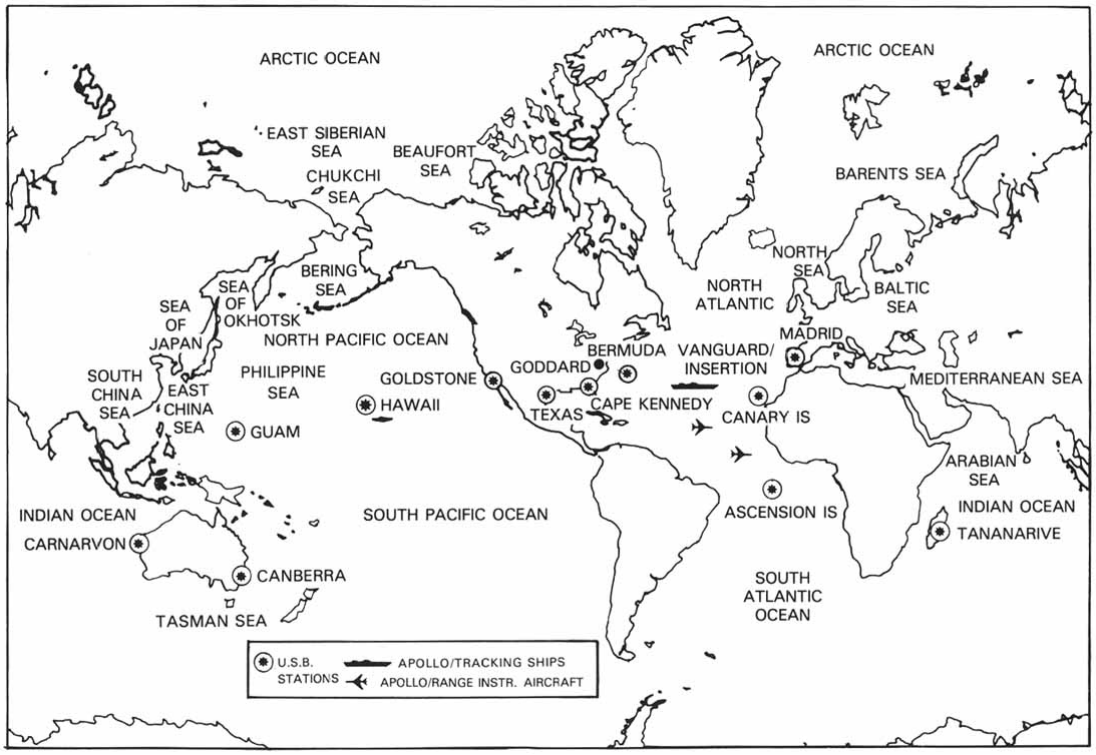

Figure 1: Apollo Manned Space Flight Network

Table 1: Apollo Station Locations

Site	Acronym	Latitude (deg)	Longitude (deg)
Canberra	DSS45	-35.4	148.98
Goldstone	DSS15	35.33	-116.9
Madrid	DSS65	40.45	-4.17
Ascension Island	ASCC	-7.95	-14.58
Bermuda	BERM	32.25	-64.83
Canary Island	CANA	27.73	-15.6
Cape Kennedy	KSC	28.47	-80.57
Carnarvon	CARN	-24.9	113.72

Guam	GUAM	13.3	144.73
Hawaii	HAWA	22.12	-157.67
Tananarive	TANA	-19	47.3
Texas	JSC	27.65	-97.38

Modern electronics would be able to provide measurement accuracies per Table 2.

Table 2: DSN Noise and Bias

	Range (m)	Doppler (m/s)
1σ noise	1	0.06e-3
1σ bias	1	0.12e-3

This network is referred to as the "baseline" network for the purposes of this analysis.

STDN SIMULATIONN

The Spacecraft Tracking Data Network (STDN) simulation was the tool utilized in for this analysis. This simulation has assumptions on the navigation architecture, processing techniques, and environment dynamics that are summarized in the following sections.

Environment Models

Initially, the environment state is randomly perturbed based on the initial environment covariance assigned. This perturbation is calculated via a Gaussian random number generator and the square root of the covariance diagonals. The initial environment covariance was based on a 500 feet one-sigma position uncertainty and a 1 ft/s one-sigma velocity uncertainty in each inertial axis. The state perturbation was performed completely in inertial coordinates; i.e. no correlations are assigned.

The environment state in the STDN simulation tool is advanced via a fixed time step Encke-Nystrom integrator. The perturbations include gravitational accelerations from the Sun, Moon, and Earth – as well as non-spherical gravity terms from the primary body. These non-spherical gravity terms have an associated uncertainty, which is used to randomly initialize the gravity model at simulation initialization. The non-spherical gravity model was configured for a 30 x 30 field. An additional acceleration term modeled as an exponentially time correlated random variable (ECRV) is also included in the integration of the environment state. The time constant on the ECRV is 3600 seconds with a 1σ approximately 2 μg's each UVW axis.

Sensor Models

Most of the assumptions regarding the sensor models have been covered in Section entitled "Assumptions and Constraints." However, it should also be noted that the count time was configured to 60 seconds for all runs and an elevation mask of 10° was applied

Navigation Models

The initial navigation state was the initial environment state perturbed via a dispersion covariance. This dispersion covariance was based on a 5 km one-sigma position uncertainty and a 5 m/s one-sigma velocity uncertainty in each inertial axis. The off-diagonal elements were initialized to zero.

Like the environment, the navigation algorithms advanced the state with a fixed step Encke-Nystrom integrator. Once again, the perturbations were gravitational accelerations from the Sun, Earth, Moon, the navigation estimate of the unmodeled acceleration, and an 8 x 8 non-spherical gravity field.

Two navigation filter algorithms are available in the STDN simulation. The first, and most widely utilized in this study, is the linearized Kalman filter. The filter is a scalar filter and the covariance update equation had been augmented to account for suboptimal filter design. The covariance was propagated in time via the state transition matrix, which was calculated by integrating the time derivative of the state transition matrix. Note that the initial covariance utilized was a lost in space inertial covariance with a 1σ of 1000 km in each position axis and a 1σ of 10 km/s each velocity axis.

The linearized Kalman filter was designed to solve for six inertial state components and a range and Doppler bias for each ground station. Additionally, the navigation state included three inertial unmodeled acceleration values. The unmodeled accelerations in the navigation state were modeled as ECRVs with a time constant of 3600 seconds. Periodically, the reference state was "rectified" with the filtered computed deviation from the reference state. At such rectification points, the filtered computed deviation is zeroed out. The rectification occurred once every hour, in order to more emulate the expected ground data processing procedures for the CEV.

The second navigation algorithm available in the STDN simulation is a batch filtering algorithm. This algorithm is configurable to utilize a priori covariance information or none at all. Additionally, solve for parameters are also configurable. The specific utilization of the batch algorithm is discussed with each appropriate run.

TRAJECTORIES

The main trajectory utilized was the leg of the CFP-1 trajectory between TEI-2 and TEI-3. This is a highly elliptical trajectory (eccentricity > 0.8) with an inclination of approximately 141°. The radius of periapsis is approximately 191 km. Note that the TEI-3 burn occurs at or near the periapsis point. The time between the TEI-2 and TEI-3 burns is approximately 32000 seconds.

In addition to the CFP-1 trajectory, additional trajectories were provided by the flight performance team for navigation analysis. These trajectories include instances of 90° plane change, variations in time between TEI-2 and TEI-3, and TEI-3 locations at minimum, maximum, and equatorial Earth fixed latitude. While the feasibility of flying such trajectories may be called into question, the navigation team desired to examine ground navigation performance for these trajectories in order to better ascertain the navigation sensitivities to geometrical phenomenon.

METHODOLOGY

As mentioned the Introduction, the study approach was three-fold:

1. A heuristic study on ground station geometrical impacts to navigation
2. A comparison between Deep Space Network only navigation performance and Apollo Manned Spaceflight Network navigation performance
3. An examination of additional "worst-case" trajectories

For items one and two, the CFP-1 trajectory was utilized. Item three is a survey of the additional trajectories described in the previous section.

Based on reference XXXX, the orbital elements of interest in preparation for the TEI-3 maneuver are the semi-major axis, inclination, longitude of ascending node, and radius of periapsis. Therefore, a good

performance measure for this analysis is the ability to resolve these Keplerian elements as compared to some baseline run. For the purposes of this analysis, this baseline run is a run utilizing the baseline ground station architecture and the linearized Kalman filter.

For runs utilizing the linearized Kalman filter, the STDN linearized Kalman filter covariance has been shown to be a statistical over-estimation of the true navigation uncertainties (ref XXXX). Therefore, a single run of the linearized Kalman filter with covariance analysis is sufficient in these cases.

Conversely, the batch filter covariance often under estimates the true navigation uncertainties. Therefore, to do appropriate navigation analyses, Monte Carlo runs are required for batch filter analysis.

RESULTS FOR BASELINE CFP-1

First, a baseline run of the CFP-1 trajectory utilizing the Apollo Manned Spaceflight Network architecture (with modern electronics) was performed. Figure 2 and Figure 3 display the results from this run. Note that the blue traces represent the actual navigation errors from the run and the red traces are the 1σ uncertainties from the covariance diagonals.

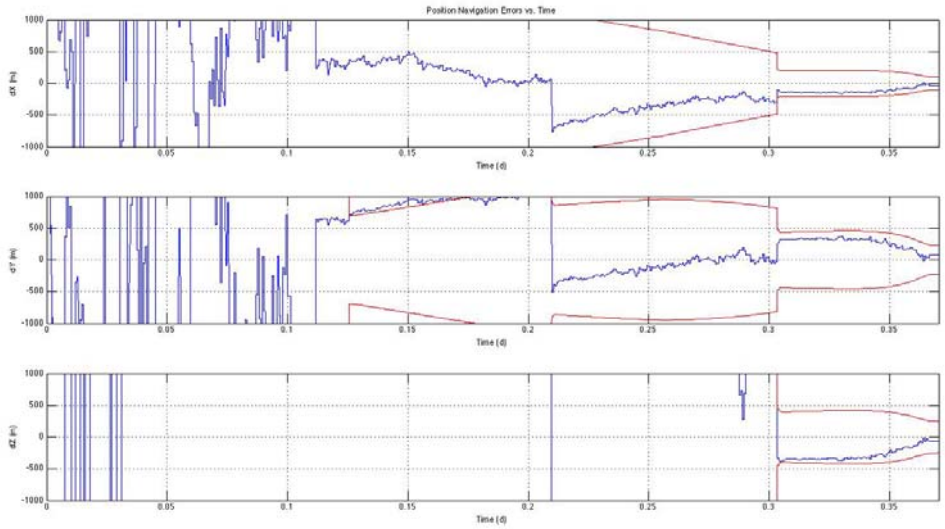

Figure 2: CFP-1 Position Errors with Baseline Ground Station Configuration

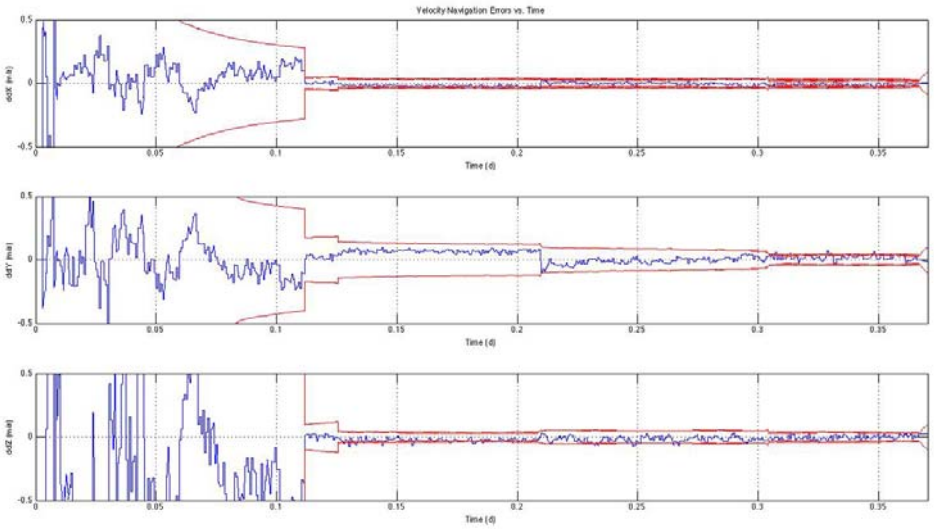

Figure 3: CFP-1 Velocity Errors with Baseline Ground Station Configuration

In the vein of the philosophy that any future navigation architecture would have similar capabilities to that of the Apollo Manned Spaceflight Network, the results of this run serves as the baseline navigation capability for ground station processing. Figure 4 maps the covariances of this run to the 1σ uncertainties for the Keplerian elements of ineterst.

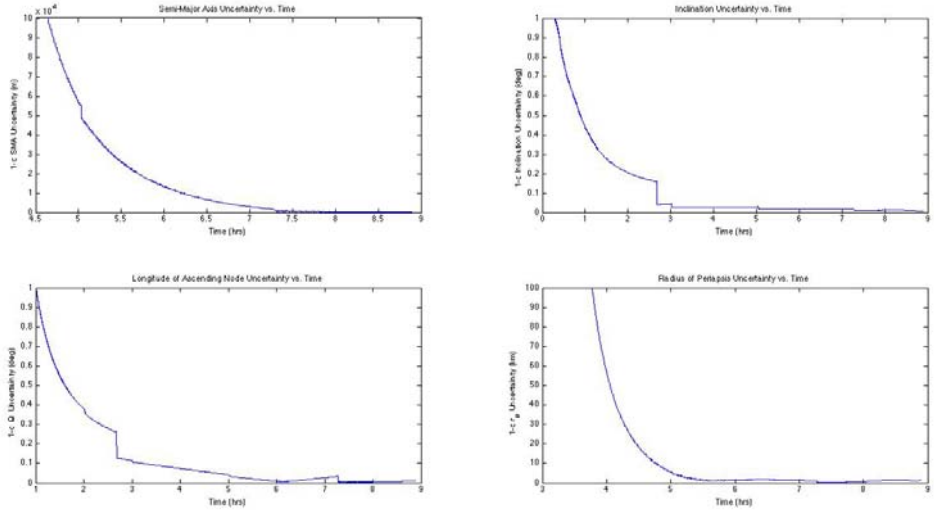

Figure 4: Local Keplerian Element Uncertainties

HEURISTIC STUDY ON GROUND STATION GEOMETRY

North-South Stations

In order to examine the sensitivities due to ground station geometry, a run of was performed utilizing DSS15, DSS45, GUAM, and an imaginary station DSS51. DSS51 is at the same longitude as DSS15 and has the same latitude as of DSS15, but is located in the Southern hemisphere. Note that this composes a ground station architecture with two stations in the Northern hemisphere with “mirror” stations (similar

longitude, but in Southern hemisphere) in the Southern hemisphere. In other words, the baseline between ground stations is perpendicular to and intersects the equator. This run was performed utilizing 3-way data with only one slave.

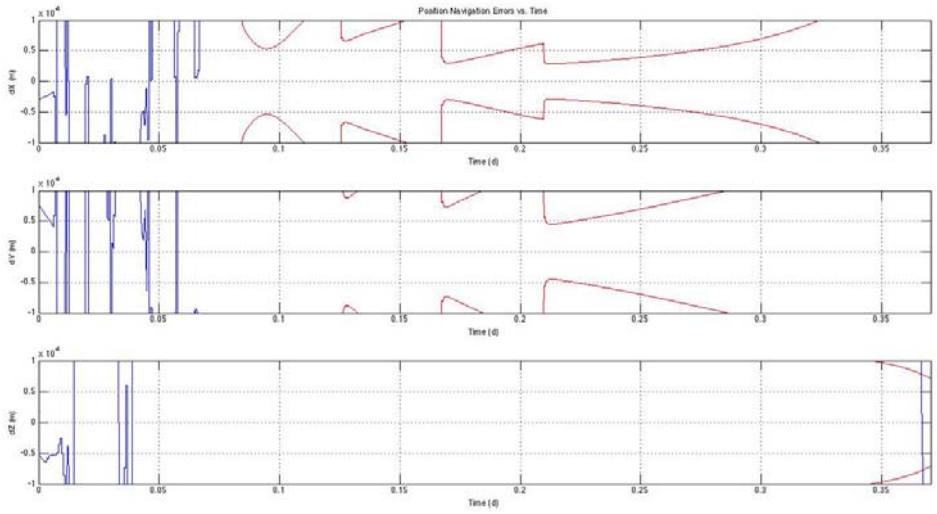

Figure 5: CFP-1 Position Errors with North-South Ground Station Configuration

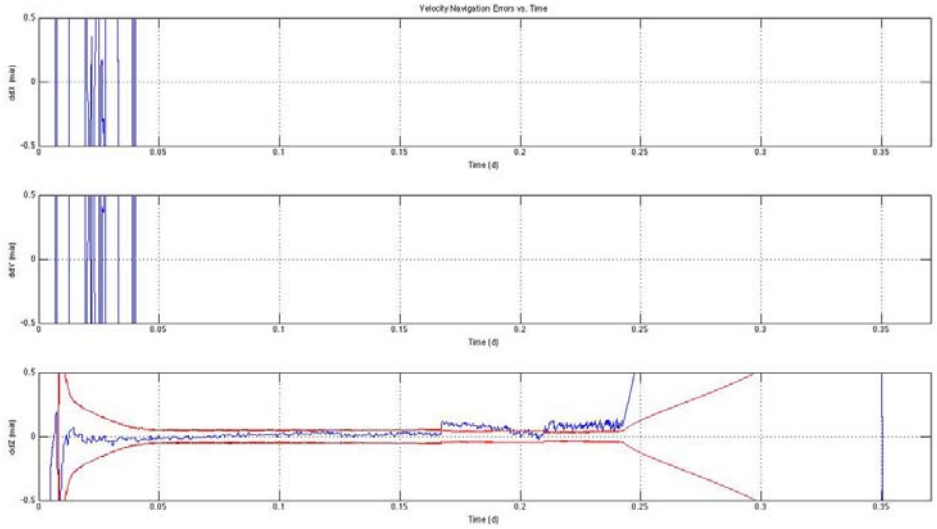

Figure 6: CFP-1 Velocity Errors with North-South Ground Station Configuration

From the results displayed in Figure 5 and Figure 6, it is clear that while processing data from ground station configuration does not let the filter to converge, it does has observability into the inertial Z axis. However, one may infer a latitude dependency on this observability. As the baseline between the two stations decreases, that is as each station moves towards the equator, the ability to resolve the Z-axis diminishes. For example, the worst case scenario is both stations located on the equator. In this case, as the stations would have the same longitude, they are co-located and therefore have zero baseline and no observability into the Z-axis. Conversely, if the two stations were located at the North and South poles, they would have maximum baseline and excellent observability into the Z-axis.

Equatorial

Another run was performed this time with a completely imaginary ground network consisting of six stations located on the equator and equally spaced in longitude. In other words, the baseline between ground stations runs along the equator. Again, for this run, only one slave was utilized for 3-way processing.

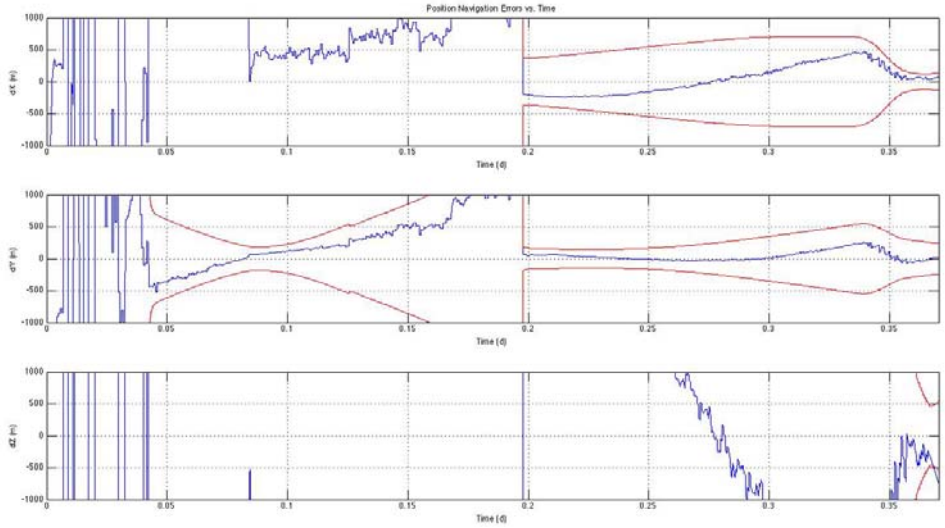

Figure 7: CFP-1 Position Errors with Equatorial Ground Station Configuration

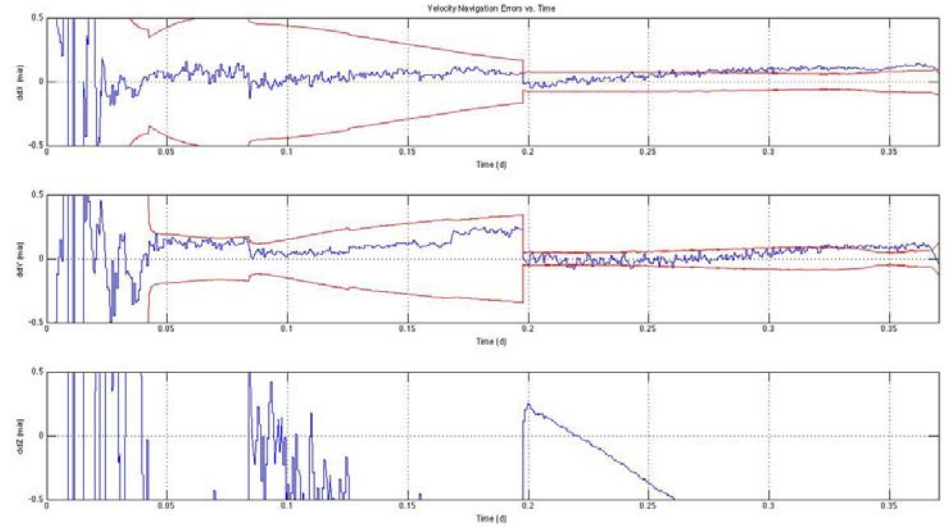

Figure 8: CFP-1 Velocity Errors with Equatorial Ground Station Configuration

Clearly, Figure 7 and Figure 8 demonstrate that the equatorial ground station configuration has strong observability in the inertial X and Y axes, but is weak in observing the Z axis. One would expect these results based on the conclusion from Section 0 where a North-South station configuration has strong observability in the Z-axis but weak observability in the X-Y plane.

As in the run described in Section 0, a latitude dependency can be inferred from this run. Imagine the entire network moves north in latitude. As the network moves North, the baseline between the stations starts to decrease. At the extreme, the network exists on the North Pole and is entirely co-located there. In this case, there is no baseline between stations and observability is limited. Therefore, the best observability in the X-Y plane is achieved when the ground network is located along the equator.

Based on the results of these two runs, one can conclude that the most optimal ground station configuration is concurrent tracking from a "cross" of stations (two stations in the Northern hemisphere and two stations in the Southern hemisphere).

Staggered Network

Based on the conclusion in the previous section, where a cross of stations about the equator is determined to be the optimal geometry for navigation, it is a reasonable assumption that a "staggered" network of stations can replicate these results. A staggered network would consist of 6 stations, equally spaced in longitude about the Earth, but alternating in latitude. That is, the magnitude of each station latitude is the same, but alternating in either Northern or Southern hemisphere. The idea being that such a geometry would simultaneously give observability to the Z-axis and the X-Y plane. To test this assertation, a third imaginary network was constructed with a latitude magnitude equivalent to that of DSS15. Again, a single run for this "staggered" network was performed with 3-way tracking utilizing a single slave.

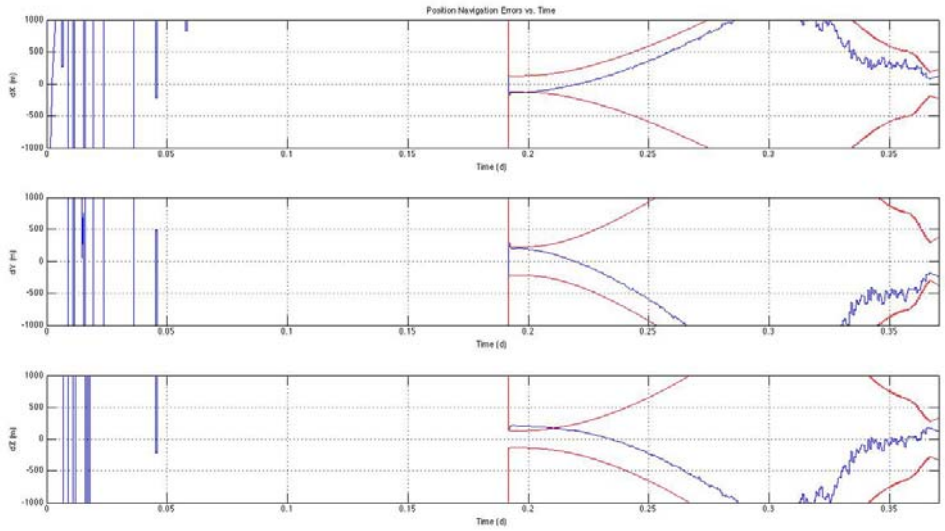

Figure 9: CFP-1 Position Errors with Staggered Ground Station Configuration

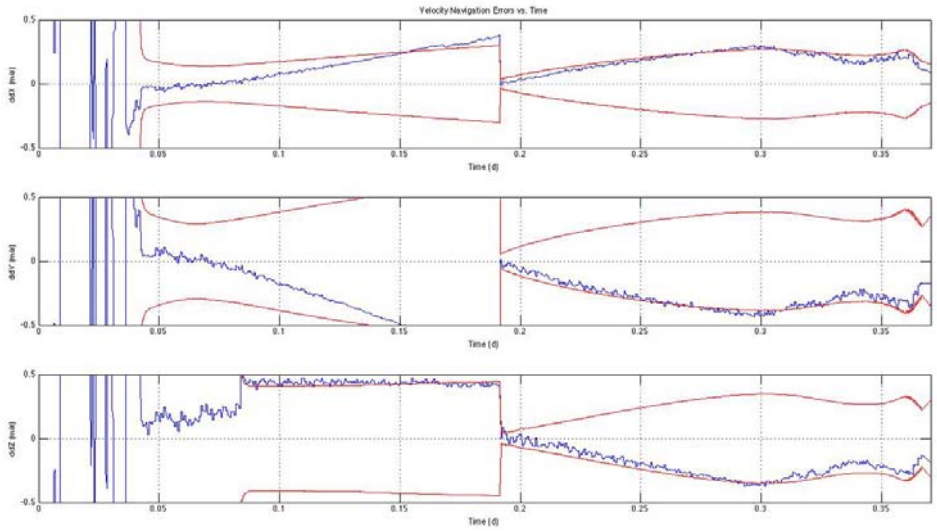

Figure 10: CFP-1 Velocity Errors with Staggered Ground Station Configuration

The remarkable observation from Figure 9 and Figure 10 is that given enough time, the staggered ground station configuration gives comparable results to the baseline run but with only one slave as opposed to two. For completeness, the same run with the staggered ground station configuration was performed this time utilizing two slaves.

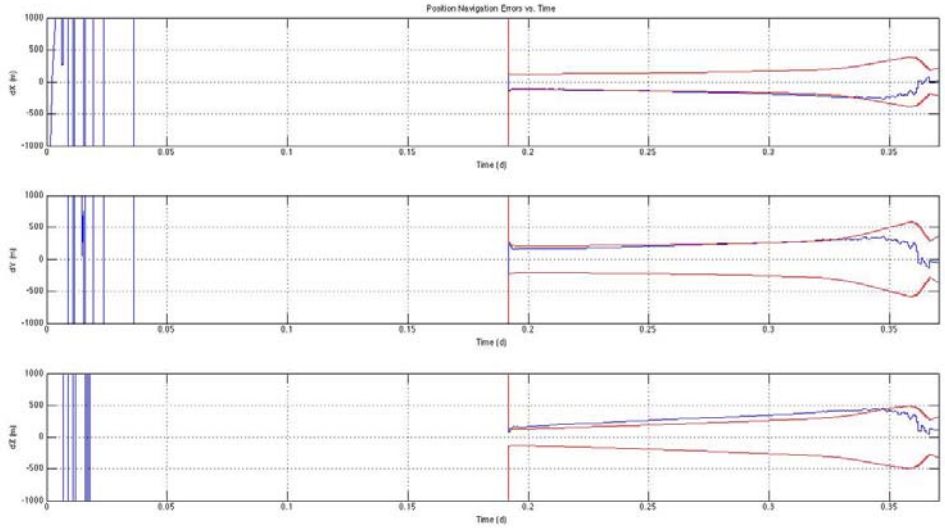

Figure 11: CFP-1 Position Errors with Staggered Ground Station Configuration and Two Slaves

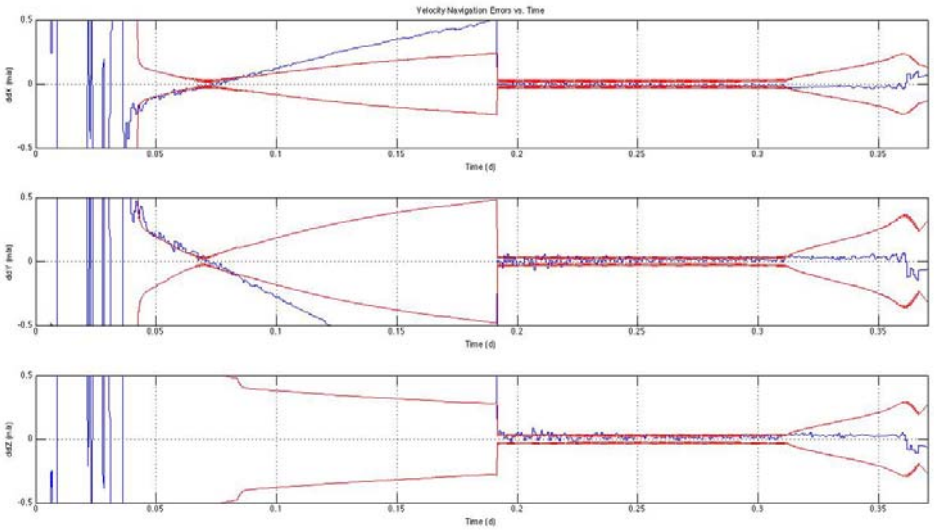

Figure 12: CFP-1 Velocity Errors with Staggered Ground Station Configuration and Two Slaves

While the baseline run from has a much smother solution, Figure 11 and Figure 12 demonstrate position and velocity accuracies more accurate than the baseline when filter convergence is achieved. Therefore, a ground network configuration with more accuracy but fewer stations has been derived – however, an exhaustive examination of all trajectories has not been conducted. **Error! Reference source not found.** maps the covariances from this run to 1σ uncertainties of the desired Keplerian elements. The baseline run is also plotted for comparison.

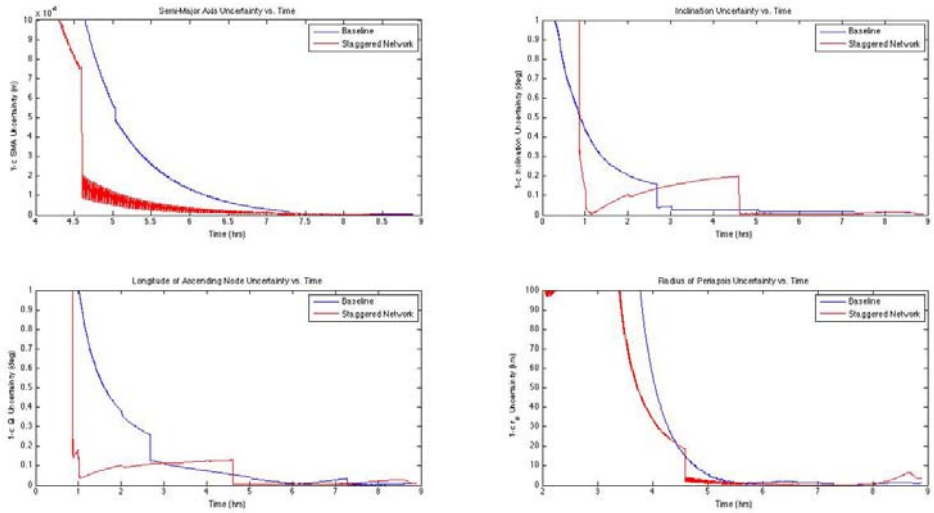

Figure 13: Staggered Network Local Keplerian Element Uncertainties

DSN ONLY PERFORMANCE

DSN Only Performance Utilizing a Linearized Kalman Filter

Next, an examination of the navigation performance when utilizing only the current DSN infrastructure (DSS15, DSS45, and DSS65) in a 3-way tracking mode was conducted. Clearly, from Figure 14 through Figure 15 the navigation solution was never able to converge and as measurement processing continued to shrink the covariance, the filter diverged as residual edits inhibited future processing. Note that other processing techniques, such as batch, may mitigate this issue.

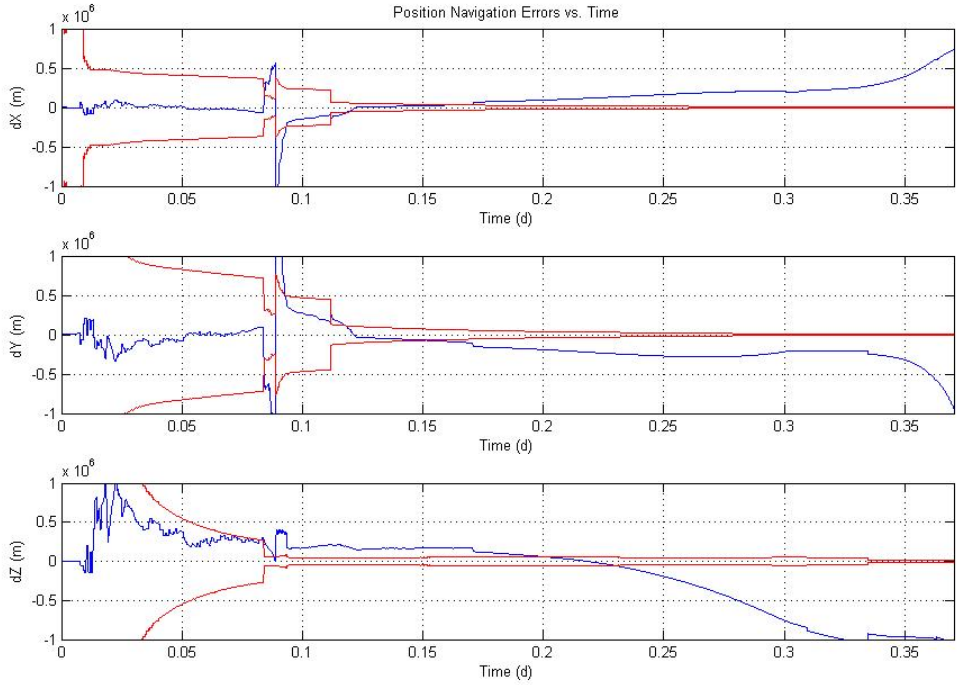

Figure 14: CFP-1 Position Errors with DSN Only Ground Station Configuration

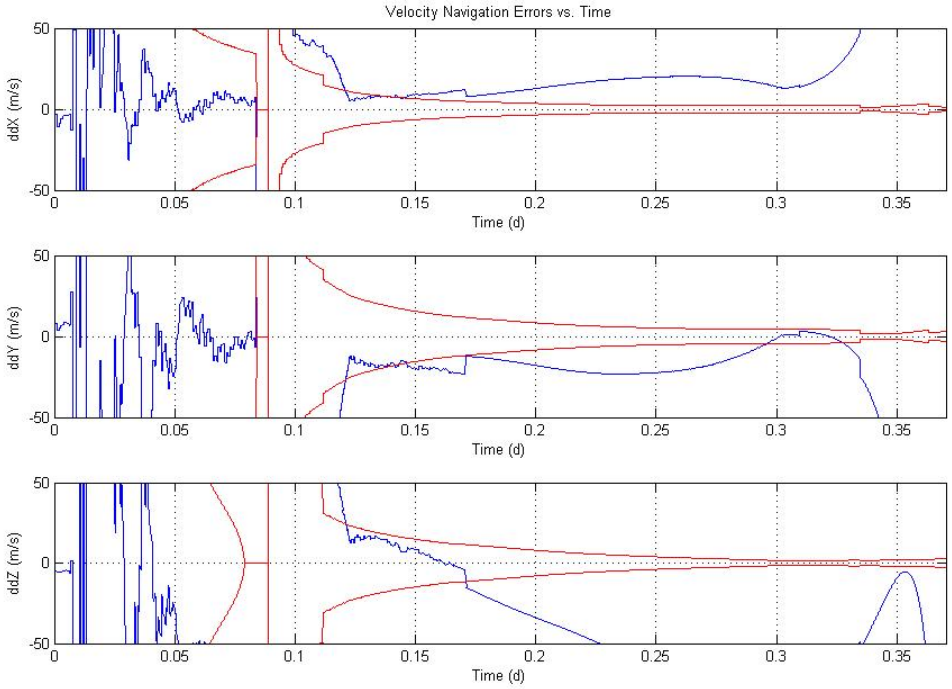

Figure 15: CFP-1 VELOCITY Errors with DSN Only Ground Station Configuration

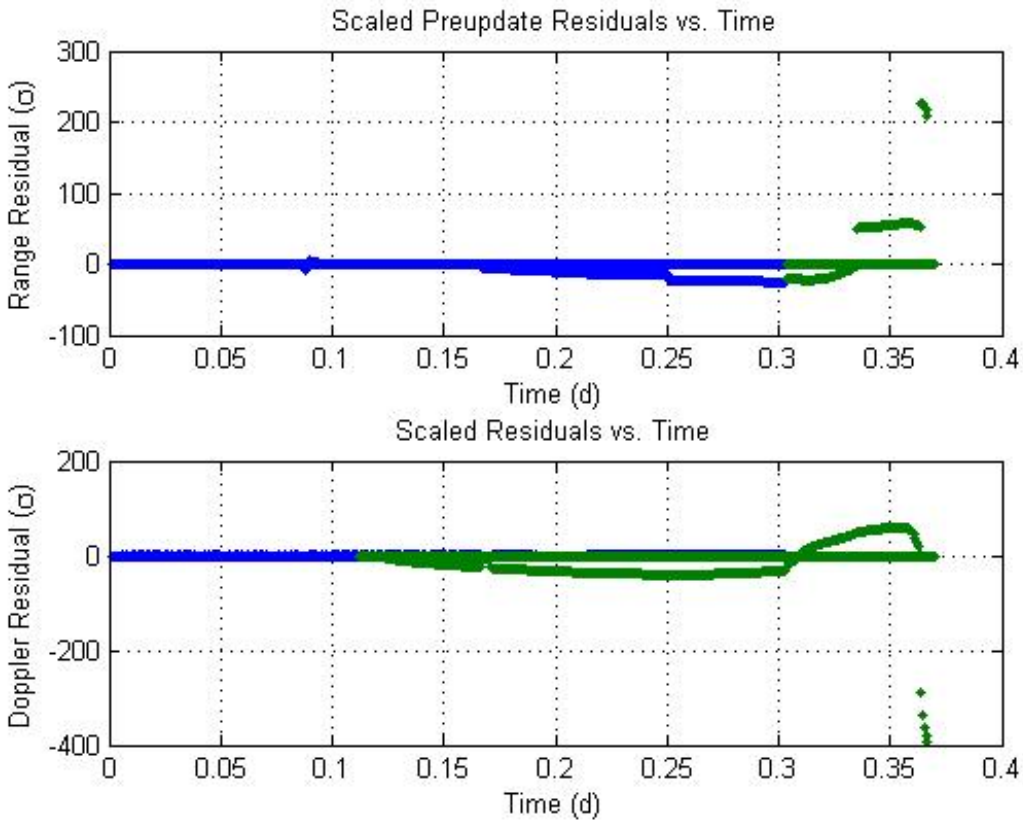

Figure 16: CFP-1 Scaled Residuals for DSN Only Ground Station Configuration

DSN Only Performance Utilizing a Linearized Kalman Filter and A Priori Knowledge

In order to demonstrate how a priori knowledge of the state and covariance can allow for effective utilization of DSN only data, a second run of the CFP-1 trajectory processing only DSN data was performed this time with significant a priori knowledge of the state and covariance. Table 3 compares the lost in space run to the a priori knowledge run.

Table 3: Lost in space vs. a priori knowledge simulation runs

	Lost in Space	A priori knowledge
Environment state dispersions	Enabled	Disabled
Navigation state dispersions	Enabled	Disabled
Position covariance (each inertial axis)	1e6 km^2	100 m^2
Velocity covariance (each inertial axis)	100 km^2 / s^2	1e-4 m^2 / s^2
Unmodeled acceleration covariance (each inertial axis)	1 m^2 / s^4	4e-10 m^2 / s^4
Unmodeled accelerations	On	On
Dispersed gravitational coefficients	On	On

Note that even though there is substantial a priori knowledge, there is still significant mis-modeling of the dynamics via the unmodeled accelerations and the randomly dispersed gravitational coefficients. Therefore for the case of measurement processing disabled, the RSS position and velocity errors would grow to about 1887 meters and 1.1238 meters per second. Figure 17 and Figure 18 illustrate the results of processing DSN only measurements with substantial a priori knowledge.

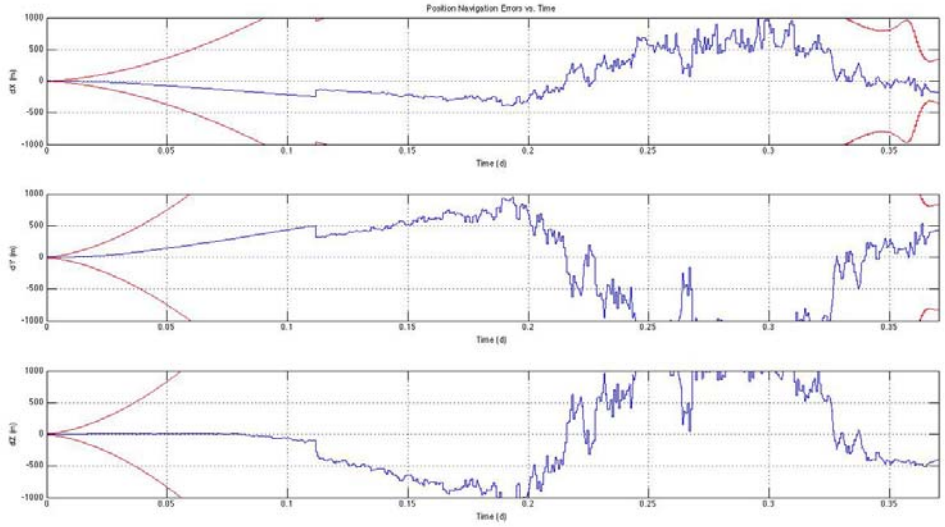

Figure 17: CFP-1 Position Errors with DSN Only Ground Station Configuration and Constrained Covariance

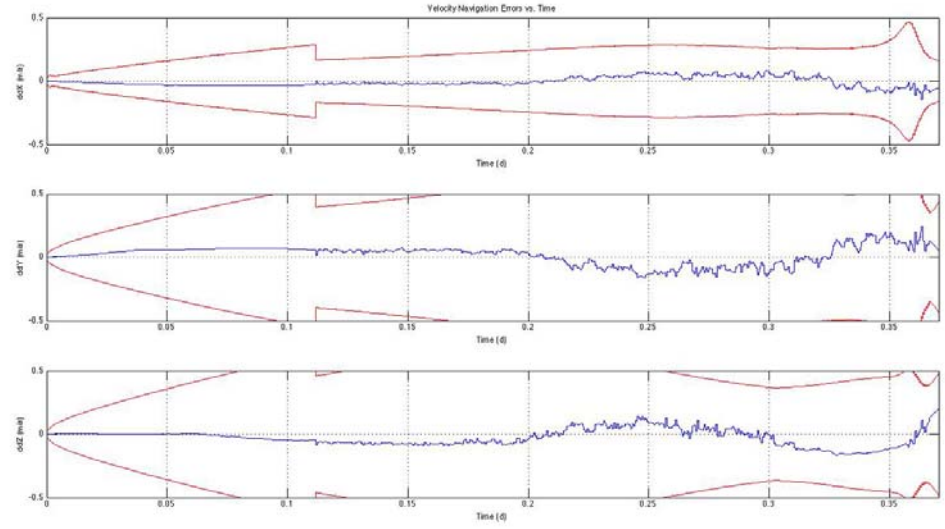

Figure 18: CFP-1 Velocity Errors with DSN Only Ground Station Configuration and Constrained Covariance

As the final navigation errors in the a priori knowledge run are less than then navigation errors from no measurement processing, *DSN only processing has been shown to mitigate the errors due to mis-modeled dynamics – if there exists sufficient a priori knowledge of the state*. Therefore, DSN only processing (or potentially fewer stations) has its place when there is sufficient a priori knowledge of the state. This could be potentially useful post TLI (where GPS can be used prior to TLI to acquire an accurate state) or coupled with other measurement processing (ie, optical navigation). However, DSN only processing has been shown to have issues with a lost in space covariance.

It should be noted again that other processing techniques, such as batch, may improve the feasibility of DSN only processing.

DSN Only and Batch Filter

For completeness, it is desirable to examine the performance of DSN only tracking utilizing a batch filter. To do so, several runs were conducted with different configurations of the batch filter in order to determine the optimal configuration. During these runs, it was noted that the batch filter had difficulties solving for biases and un-modeled accelerations without significant a priori state knowledge. Additionally, the batch filter would not converge in 10 iterations for short arc solutions. Based on these runs, a 100 run Monte Carlo was performed that utilized no a priori covariance and broke the tracking arc between TEI-2 and TEI-3 into two "batches". This corresponds to batches of length about 4.4 hours. The batch filter coupled with the DSN only solution was incapable of converging for tracking arcs shorter than 4.4 hours. Therefore, the DSN only configuration was unable to generate short arc solutions less than 4.4 hours. The batch filter was also configured for a state only solution, ie no solve for parameters other than inertial position and velocity. Since there were no solve for parameters, the navigation measurement covariance was increased to swamp the effects due to measurement bias. For completeness, the same 100 run Monte Carlo was performed utilizing the baseline network as well. The results of these two runs and the baseline run are plotted in Figure 19.

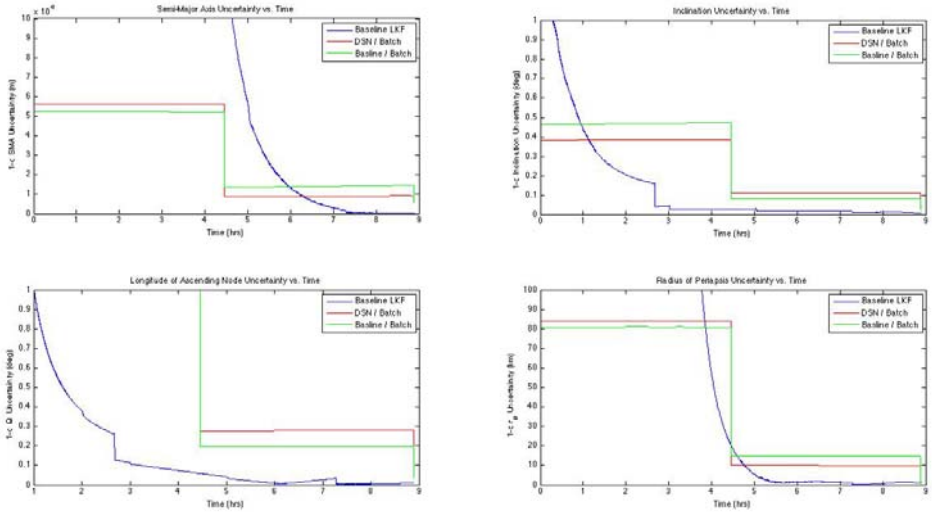

Figure 19: Baseline and Batch Filtering Local Keplerian Element Uncertainties

Note that the initial navigation dispersions correspond to 3σ uncertainties over 1° in planar resolution and an uncertainty on whether or not Orion will crater into the lunar surface (radius of periapsis 3σ uncertainty is larger than the actual radius of periapsis).

Figure 19 remarkably does not show marked improvement in the navigation state when comparing the baseline network performance to that of DSN only. However, the baseline run from is nearly an order of magnitude improved in all Keplerian elements by the end of the run. In order to illustrate what is occurring, another 100 run Monte Carlo of batch filtering the baseline network was performed this time with the tracking arch broken up into 5 batches (ie, each batch is approximately 1.75 hours long). Recall that the DSN only network was incapable of generating such short arc solutions. Figure 20 is Figure 19 with this new run overlaid.

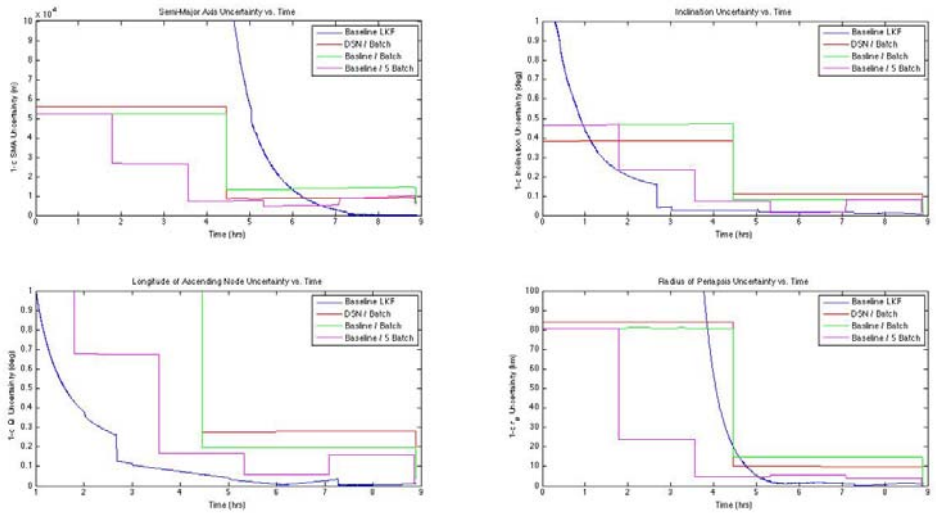

Figure 20: Baseline and Batch Filtering Local Keplerian Element Uncertainties

Clearly, a distinct advantage of the baseline network over the DSN only network is the ability to generate short arc solutions. For example, from Figure 20, the baseline network is able to determine the need to perform an altitude adjust maneuver in less than 2 hours, while the DSN only solutions require 4.4 hours. This is could be a substantial benefit for emergency or off-nominal operations.

ADDITIONAL TRAJECTORY RUNS

OPS-1 – OPS-5 Trajectories

The OPS-1 – OPS-5 trajectories were an attempt to characterize the "worst-case" trajectories. These trajectories include 90° plane change in lunar orbit to achieve the desired departure asymptote and shortened time periods from TEI-2 to TEI-3. Table 4 lists the Keplerian elements for each of these trajectories.

Table 4: KEPLERIAN ELEMENTS FOR OS TRAJECTORIES

	Time Between TEI-2 and TEI-3 (seconds)	SMA (km)	Eccentricity	Inclination (degrees)	Radius of Periapsis (km)	Longitude of Ascending Node (degree)
CFP-1	32000	9.7893e+03	0.8021	141.1032	199.1844	142.4031

OPS1	23780	1.2453e+04	0.8531	52.8716	91.6291	142.9558
OPS2	24010	1.2239e+04	0.8501	43.1984	96.3270	339.6656
OPS3	23840	1.2795e+04	0.8564	84.4554	99.7524	68.2332
OPS4	23520	1.2607e+04	0.8505	100.2807	146.4296	26.7988
OPS5	23190	1.2418e+07	0.8487	22.8192	140.2370	312.1512

Each of these trajectories was processed utilizing the baseline network with 1 master and two slave stations. **Error! Reference source not found.** plots the performance of these trajectories and the CFP-1 trajectory as well.

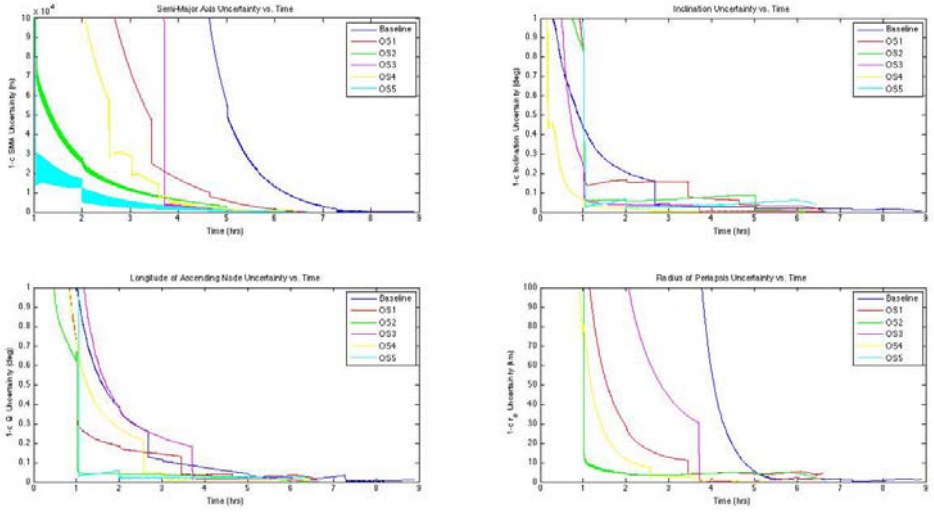

Figure 21: OPS Trajectories Local Keplerian Uncertainties

Of note is the consistent ability of each of these OPS trajectories to converge quicker on semi-major axis and radius of perigee. This is in part due to a "spike" in the uncertainty of semi-major axis in the CFP-1 run. To illustrate this, the plot of the CFP-1 semi-major axis uncertainty from **Error! Reference source not found.** is zoomed out and shown in **Error! Reference source not found.**.

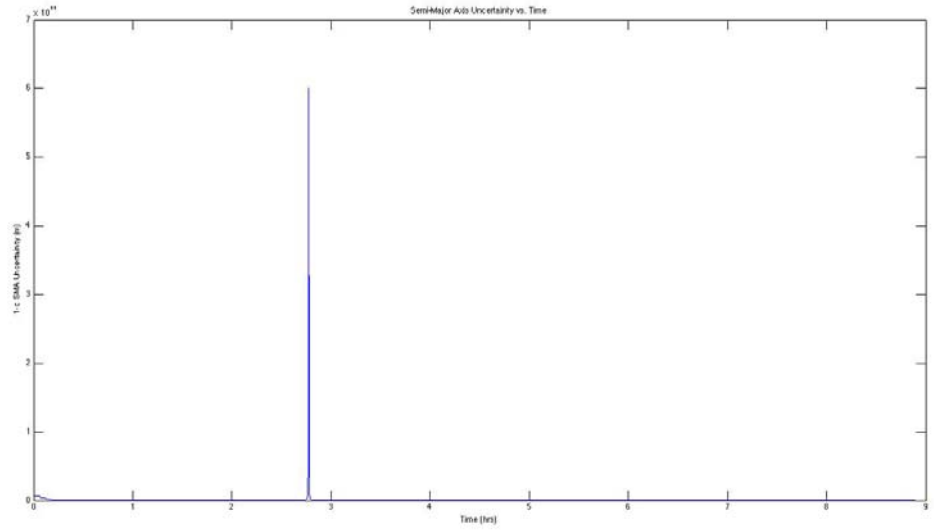

Figure 22: CFP-1 Semi-Major Axis Uncertianty

However, from the position and velocity error plots in Figure 2 and Figure 3, which are relatively smooth, this type of spike is unexpected. The source of this spike is due to a torquing of the covariance correlations at a station change. Figure 23 plots the out-of-plane position / downtrack velocity correlation coefficient for the baseline and OPS-5 trajectory run.

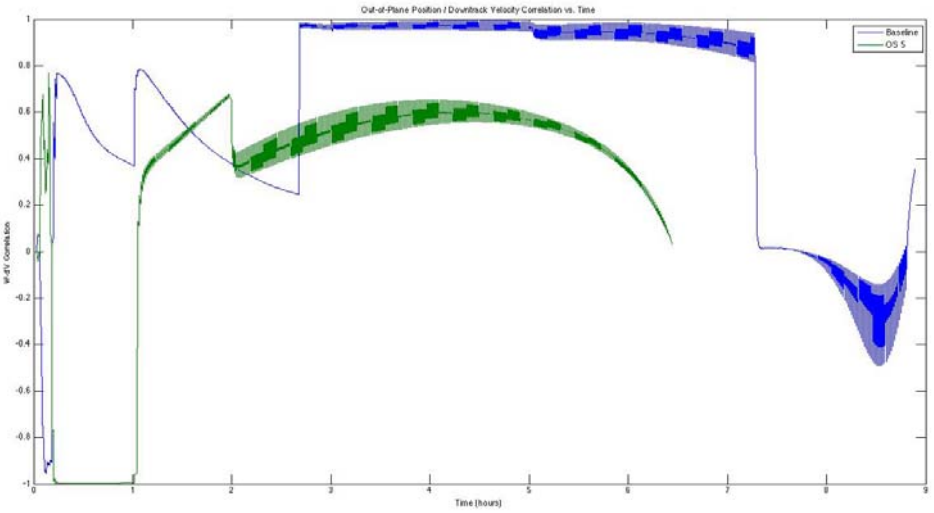

Figure 23: Out-of-Plane / Downtrack Velocity Correlation Coefficient

As downtrack velocity and out-of-plane position are uncorrelated in elliptical orbits, one would expect these correlations to be small. Note that for the baseline run, the covariance matrix demonstrates a strong correlation for these elements corresponding to the time of the semi-major axis uncertainty spike. Also note that for the OPS-5 trajectory, when the correlation jumps to small values from -1, that corresponds to the quickiest decrease in radius of periapsis uncertainty.

It would certainly appear that for these highly elliptical trajectories where a lost in space condition occurs near the apoapsis, the capability of the navigation system is improved as the Orion moves closer to periapsis. It is also worth noting that the worst case flight performance trajectories do not necessarily translate into the worst case navigation trajectories. That is, as the Orion traverses along the straight-line portion of the trajectory, it is difficult to appropriately determine the correct correlations in the covariance and navigation performance may suffer. Conversely, as the geometry of the trajectory improves, the ability to determine the correlations increases and so does navigation performance.

A special note should be made about the OPS4 and OPS5 trajectories. For both of these trajectories, the TEI-3 maneuver occurs in the Earth's Southern hemisphere and DSN only tracking would not be able to provide continuous tracking. To illustrate this consider Figure 24 which plots the OPS-5 range edit flags.

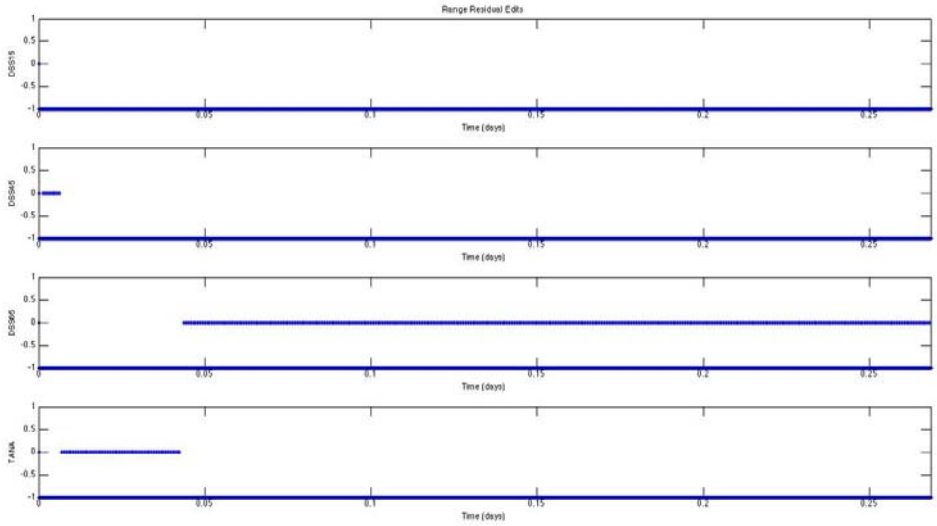

Figure 24: Range Edit Flags for OPS-5 (-1 = not available, 0 = data processed, 1 = 3σ residual edit)

Note that TANA is required to be the master to provide continuous tracking for OPS-5. Since TANA tracking occurs near the beginning of the simulation, the operational ability of the DSN to confirm the TEI-2 burn is called into question. *In addition, with the demonstrated inability of the DSN only solutions to perform short arc solutions, data gaps such as this one, calls into question the feasibility of the DSN only network to adequately target the TEI-3 burn for trajectories with shortened time periods between TEI-2 and TEI-3.*

Maximum, Zero, and Minimum Latitude

To further investigate the sensitivity of the navigation performance due to the location of the TEI-3 maneuver in terms of Earth fixed latitude, the flight performance team generated three trajectories where the TEI-3 maneuvers occurred at maximum, zero, and minimum Earth fixed latitude (reference XXX). These three trajectories were then processed utilizing the baseline network. Because of the uniqueness of these trajectories, the restriction of two slaves was restricted, i.e. every station in view generates a measurement that is processed. Figure 25 displays the results for these trajectories.

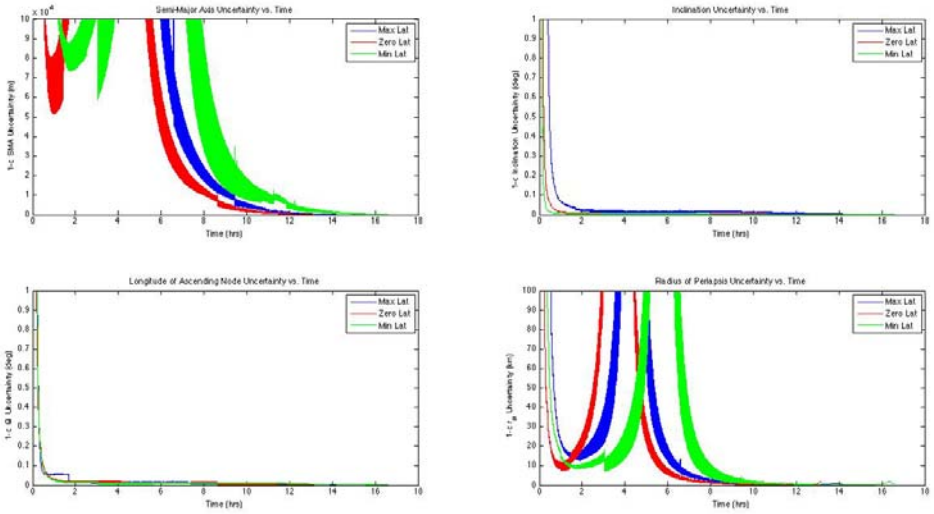

Figure 25: Local Keplerian Uncertainties for Minimum, Zero, and Maximum Latitude

Note that these three trajectories are significantly longer in time duration than what has been seen before. As such, they exhibit the spike in semi-major axis illustrated in the previous section, essentially confirming the observation that navigation performance can be adversely affected by trajectory geometry.

As the baseline architecture is optimized about the equator, one would expect (as observed from **Error! Reference source not found.**) that the zero latitude trajectory exhibits the best performance. Additionally, as the baseline architecture is unbalanced such that more stations are in the Northern hemisphere, one notices that the navigation performance of the maximum latitude trajectory is superior to that of the minimum latitude trajectory. As in the case of the OPS-4 and OPS-5 trajectories, the minimum latitude trajectory cannot have continuous tracking from a DSN only network (see Figure 26).

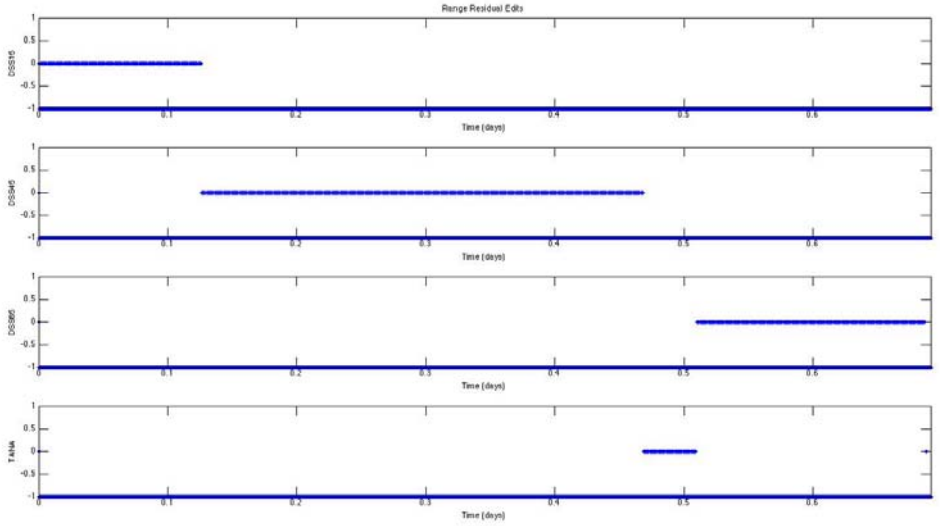

Figure 26: Range Edit Flags for Minimum Latitude trajectory (-1 = not available, 0 = data processed, 1 = 3σ residual edit)

SUMMARY AND CONCLUSIONS

In this analysis, several runs using the STDN simulation have been conducted. First, a baseline run was performed in order to characterize the expected navigation performance at TEI-3.

After that, an examination of ground station geometrical impacts was conducted. It was shown that two stations located at the same longitude but mirroring in latitude from Northern and Southern hemispheres provide excellent observability in the inertial Z-axis but no observability in the X-Y inertial plane. Conversely, a ground station configuration where all stations are located on the equator provided excellent observability into the X-Y plane, but no observability in the inertial Z-axis. Based on these results, it was concluded that the optimal ground station geometry for navigation was concurrent tracking from four stations that form a cross (two stations in the Northern hemisphere and two in the Southern hemisphere).

Based on this conclusion, a hypothesis was proposed that a staggered configuration of stations (six stations equally spaced in longitude and alternating between Northern and Southern hemisphere locations) would provide the same observability as a square ground station configuration. It was shown that given enough time that such a configuration would provide comparable results to the baseline run with one slave and would also provide more accurate results than the baseline with two slaves. Additionally, it should be noted that since TEI-3 is primarily an energy change burn, observability of the energy of the orbit would be eliminated in the case where the plane of the orbit is normal to the ground station baseline with a staggered ground network configuration. Mitigation for this case can be accomplished by utilizing two slaves instead of one. Utilizing two stations may also be desirable to protect for station failure scenarios – that is, making ground navigation 1 fault tolerant at the station level.

Note that implementation of such a 6 station staggered network might not be possible due to landmass constraints (note the lack of land in Pacific ocean), geo-political constraints, or financial constraints but the author is confident that such a network would be the optimal with respect to navigation performance. Also note that such a network has not been tested with an exhaustive set of trajectories.

Next, the feasibility of using a DSN only network was examined. It was found that the current navigation architecture in the STDN simulation (linearized Kalman filter) was unable to converge to a solution. However, with sufficient a priori knowledge, a DSN only ground configuration was demonstrated to mitigate the effects due to lunar gravitational uncertainty and unmodeled acceleration. Potential applications of this may include the time period after TLI (where GPS was utilized to achieve accurate a priori knowledge of the state) or coupling ground station data with optical navigation.

Returning to the lost in space scenario, Monte Carlo runs utilizing batch techniques were performed. From these runs, it was found that the main advantage of the baseline network over the DSN only network was the ability to do short arc solutions. The DSN network was unable to converge for arcs less than 4.4 hours, while the baseline network was able to provide critical information in less than 2 hours.

Finally, an examination of other trajectories was conducted. It was found that navigation performance can deteriorate during the straight line portion of the highly elliptical trajectories. In addition, it was also demonstrated that the DSN only network is incapable of providing continuous communications and tracking for trajectories located in the Earth's Southern hemisphere. Coupled with the DSN only network's inability to perform short arc solutions, the feasibility of the DSN only network to target TEI-3 for certain trajectories is of concern.

REFERENCES

1. J. L. Doe and J.W. James, "The Parameterization of Rotation," *Nonlinear Dynamics*, Vol. 32, No. 3, 2005, pp. 71–92.

2. *Style Manual*, American Institute of Physics, 335 East 45th St., New York 17, New York, 2nd Edition, 1959.